Amplitude enhancement of RTM angle gathers with deconvolution

Sean Crawley, Faqi Liu, Elena Klochikhina, Nizar Chemingui and Dan Whitmore, PGS*

Summary

Deconvolution has been routinely applied in seismic processing to enhance the resolution of migrated images. While full multi-dimensional deconvolution is only achievable through computationally expensive least-squares migration, we demonstrate that, when properly implemented, the deconvolution imaging condition can efficiently improve the image resolution and produce more balanced angle gathers. Using both synthetic and a field data examples, we demonstrate the enhancement in the amplitude of the migrated images and angle gathers using a deconvolution imaging condition.

Introduction

Reverse time migration (RTM) has been established as the preferred imaging solution in complex regimes. The algorithm constructs an image by applying a proper imaging condition to a forward propagated source wavefield with a reverse extrapolated receiver wavefield, both along the time axis. Conventionally, the imaging condition is cross correlation-based.

As the demand for improved resolution increases, the quest for better amplitude fidelity is highly desirable as well. By solving for a reflectivity model that minimizes the difference between a modeled data with the field one, least-squares reverse time migration has been acknowledged to be capable of deriving higher resolution images. This inversion can be implemented either in data domain as an iterative process or in the image domain known as migration deconvolution (Yu, et al. 2006). Even though the migration deconvolution is much cheaper compared to the iterative approach, it still requires to solve the inverse of a Hessian matrix, which can be computation demanding for a large scale dataset.

The deconvolution imaging condition has long been known to improve the resolution and produce amplitudes that are more directly related to the reflection coefficient (Claerbout, 1971). This imaging condition has been widely employed in one way wave equation migration, but rarely implemented in RTM. Nevertheless, the cross correlation based inverse scattering imaging condition (ISIC) for RTM can be efficiently extended to deconvolution based to remove the low-wavenumber artifacts (Crawley et al., 2018). Even though it is often found being inferior to the inversion based algorithms, this deconvolution based imaging condition can in deed uplift the image quality by compensating for the source side illumination and produce more AVA compliant angle gathers.

Using both synthetic and field datasets, we demonstrate that the deconvolution imaging condition can successfully remove the low-wavenumber backscattered noise. Compared to cross-correlation based algorithm, it also produces higher resolution and more amplitude balanced angle gathers, which can be close to what we can get from the more computationally demanding migration deconvolution.

Theory

The inverse scattering imaging condition (ISIC) consists of a weighted summation of two image kernels: a cross-correlation of the source and receiver wavefields and a dot product of their gradients (Stolk et al., 2009; Wang et al., 2010; Whitmore and Crawley, 2012). These kernels correspond to equations 2 and 3 below:

$$I(\bar{x}) = \int [w_1(\bar{x},t)h_1(\bar{x},t) + w_2(\bar{x},t)h_2(\bar{x},t)]\, dt \quad (1)$$

Where,

$$h_1(\bar{x},t) = \frac{1}{v^2} R(\bar{x},t) \cdot S(\bar{x},t) \quad (2)$$

$$h_2(\bar{x},t) = \nabla\psi_R(\bar{x},t) \cdot \nabla\psi_S(\bar{x},t) \quad (3)$$

Variables S and R are the source (forward) and receiver (backward) wavefields, ψ_S, ψ_R are their corresponding wavefields filtered by ω^α, v and ω are the velocity and frequency, and w_1 and w_2 are weighting functions of time and space that are adaptively determined.

Deconvolution-based RTM imaging condition

A deconvolution-based inverse scattering imaging condition is also made of two parts, which we implement in the frequency domain:

10.1190/segam2019-3216421.1

$$I(\bar{x}) = \int \left[W_1(\bar{x},\omega) H_1(\bar{x},\omega) + W_2(\bar{x},\omega) H_2(\bar{x},\omega) \right] d\omega \qquad (4)$$

Where,

$$H_1(\bar{x},\omega) = -\frac{1}{v^2} \frac{R(\bar{x},\omega) \cdot S^*(\bar{x},\omega)}{\left\langle S(\bar{x},\omega) \cdot S^*(\bar{x},\omega) \right\rangle + \varepsilon} \qquad (5)$$

and

$$H_2(\bar{x},\omega) = \frac{\nabla \psi_R(\bar{x},\omega) \cdot \nabla \psi_S{}^*(\bar{x},\omega)}{\left\langle S(\bar{x},\omega) \cdot S^*(\bar{x},\omega) \right\rangle + \varepsilon} \qquad (6)$$

Here, W_1 and W_2 are two adaptively computed weighting functions of frequency and space variables. The brackets in the denominators stand for certain smoothing function to the power spectrum of the source wavefield. ε is a stabilizer.

Image domain least squares RTM

As a linear inversion operator, least squares migration solves for a reflectivity model that minimizes the difference between a modeled data with the field one in a least squares sense. Its objective function is

$$E(M) = |d - LM|^2 = minimum\ , \qquad (7)$$

Which has a solution as

$$M = (L^T L)^{-1} L^T d\ . \qquad (8)$$

Here, d is the field data, M is the reflectivity, L is the modeling operator, its adjoint, L^T, is the migration operator, i.e., $L^T d$ is the migrated image. Equation (8) indicates that migrated image is in fact a blurred reflectivity. The deblurring operator to the migrated image, $(L^T L)^{-1}$ also known as migration deconvolution, improves the image resolution and reduces migration artefacts by correcting for the uneven illuminations of both the source and receiver wavefields, it also mitigates the impact of incomplete acquisition. However, the deconvolution imaging condition in equations (4 – 6) mainly compensates the source side illumination variation.

Synthetic examples

We first test the algorithms use a synthetic data with known analytic solution, where the shot gather is generated from a constant velocity model with two half space of density. As expected, the reflectivity at the density interface is independent of angle. However, the cross-correlation imaging condition produces angle domain image gathers with clear amplitude decaying as angle increases (Figure 1a) because of the geometrical spreading. In contrast, the deconvolution imaging condition (Equation 4-6) corrects this variation by removing the spreading at the source side (Figure 1b). Migration deconvolution, which addresses the variation of both source and receiver wavefields, produces angle domain common image gather with more balanced amplitude across the angle axis (Figure 1c).

The velocity model of the 2nd synthetic dataset includes a large salt body (Figure 2a), and the 3 layer density model (Figure 2b) makes the interface at the bottom mainly with density contrast, thus a nearly angle independent reflectivity is expected at this interface. Figure 2c is the RTM image. The complicated top salt causes a strong illumination variation underneath, which makes the angle gathers generated using a cross correlation imaging condition having strong amplitude variation (Figure 2d). The deconvolution imaging condition compensates the source side illumination and produces a more balanced angle gathers (Figure 2e). It is closer to that produced by the inversion based migration deconvolution results (Figure 2f), which is mostly evident for the flat density interface at the bottom.

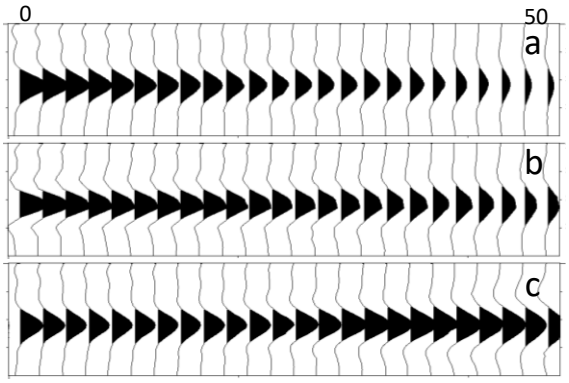

Figure 1. Angle domain RTM common image gather for data generated due to density contrast: a) from cross-correlation imaging condition; b) from deconvolution imaging condition; c) by migration deconvolution.

Field data example

We applied the algorithms to a 3D narrow-azimuth dataset collected in a salt environment. As expected, the massive salt body makes high resolution imaging underneath a challenge. Compared to the image

10.1190/segam2019-3216421.1

produced using cross-correlation imaging condition shown in Figure 3a), a deconvolution imaging condition images some events more energetically (c). In addition, the angle gathers have much more balanced amplitude across the angle axis; see b) and d). Finally, migration deconvolution improves the sharpness of the image subsalt (e) and balances the gathers (f).

Conclusions

We compare the performance of a deconvolution-based imaging condition for RTM with cross correlation based one and the inversion based migration deconvolution in terms of improving the seismic resolution and balancing the amplitude in angle domain common image gathers. We demonstrate that even though this imaging condition is not as accurate as migration deconvolution, at only 1.3x the computational cost of cross correlation, it can produce an improved image and angle gathers without as significant an increase in computational cost as least squares inversion, which costs at least 2x compared to the cross-correlation based method.

Acknowledgments

The authors would like to thank PGS for permission to publish this work.

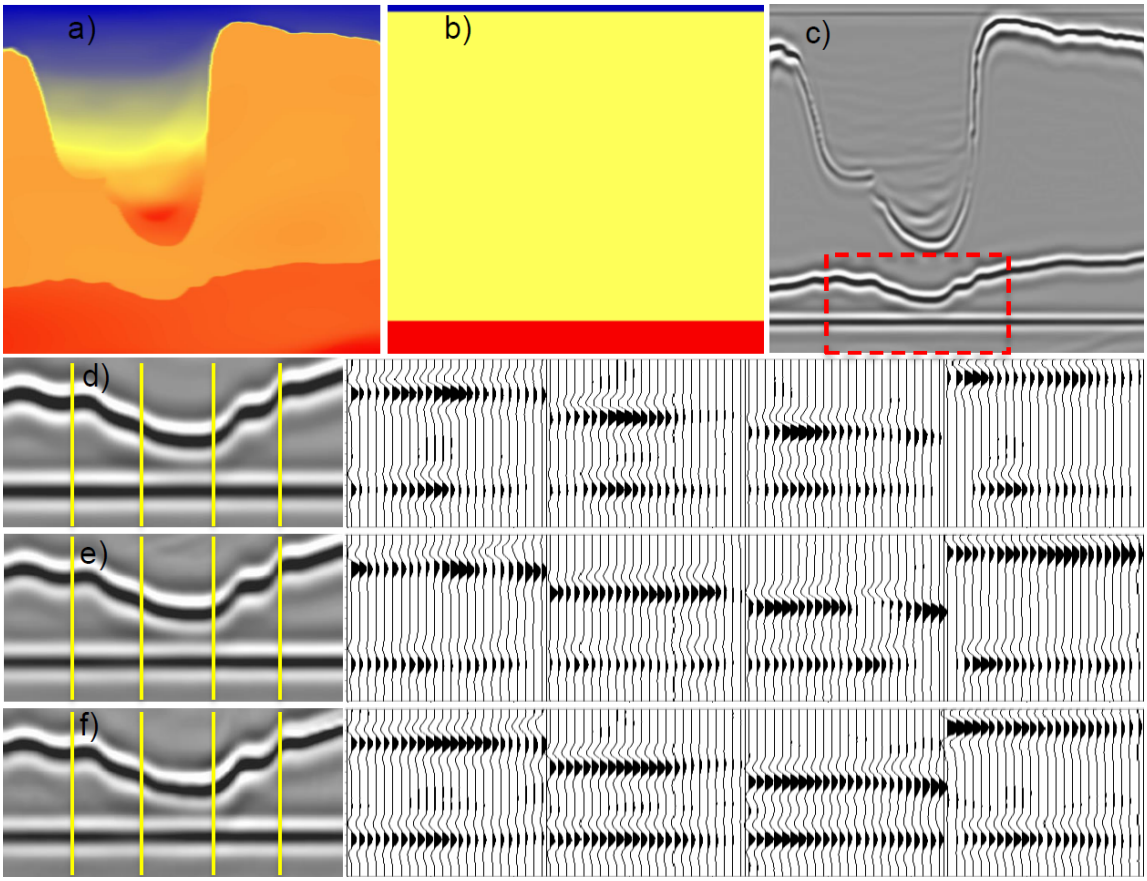

Figure 2: A synthetic example: a) the velocity model; b) the density model; c) one inline section in a migrated volume; and d), e) and f) show a zoomed portion of the images inside the box, and the RTM angle gathers from 0 to 50 degree underneath the salt body at the 4 image locations marked by the yellow lines, which are produced using a cross correlation imaging condition (d); deconvolution imaging condition (e) and migration deconvolution (f).

10.1190/segam2019-3216421.1

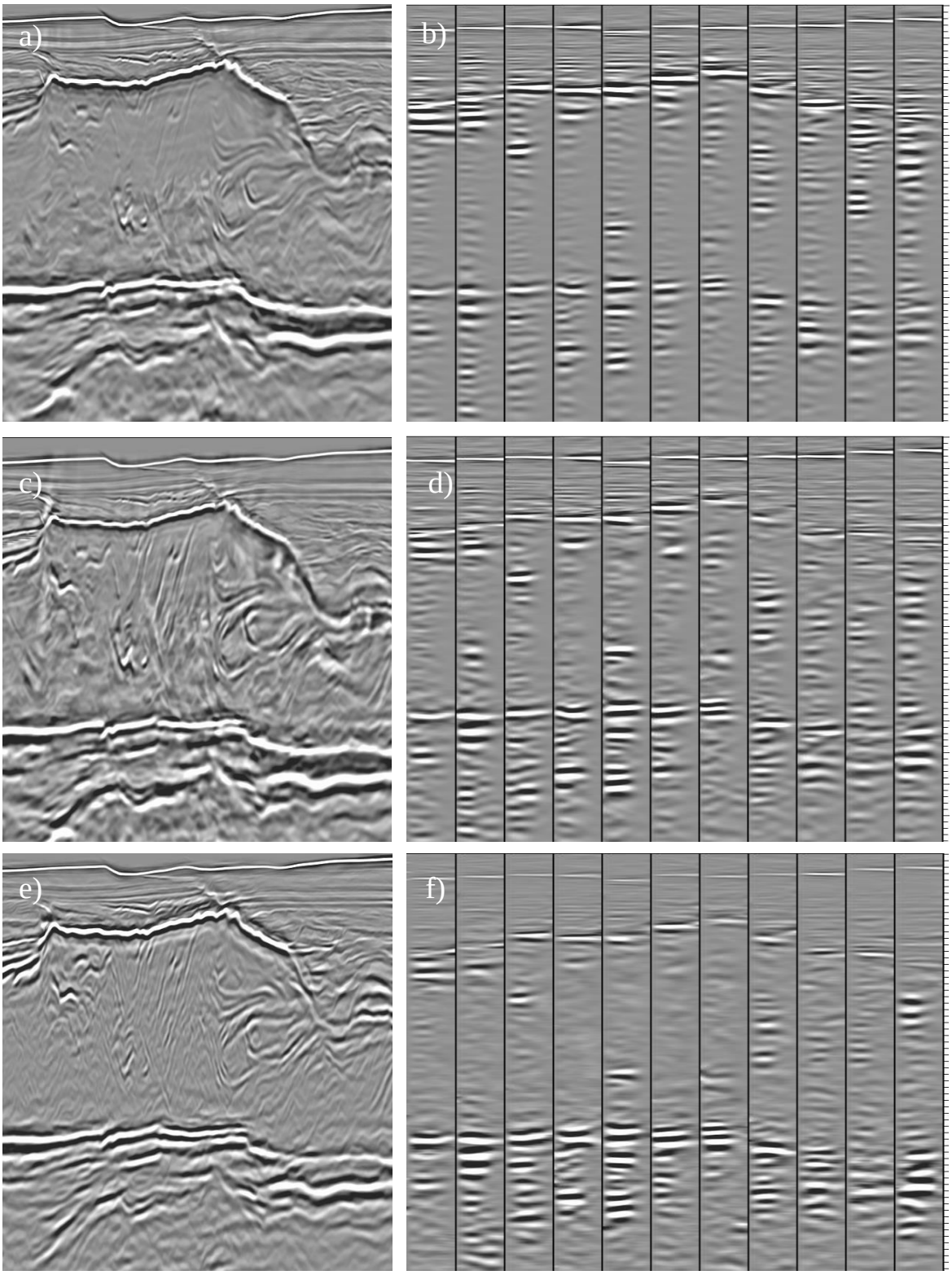

Figure 1: One inline section in a 3D RTM image using a) cross correlation; b) angle gathers of a); c) using a deconvolution imaging condition; d) angle gathers of c); e) using migration deconvolution; and f) angle gathers of e).

10.1190/segam2019-3216421.1

REFERENCES

Claerbout, J., 1971, Toward a unified theory of reflector mapping: Geophysics, **36**, no. 3, 467–481, doi: https://doi.org/10.1190/1.1440185.

Crawley, S., E., Klochikhina, and N.D., Whitmore, 2018, A deconvolution inverse-scattering imaging condition for RTM separated wavefield imaging: 88th Annual International Meeting, SEG, Expanded Abstracts, 4372–4376, doi: https://doi.org/10.1190/segam2018-2996390.1.

Stolk, C. C., M. V., de Hoop, and T., Op't Root, 2009, Linearized inverse scattering based on seismic reverse-time migration: Proceedings of the Project Review, Geo-Mathematical Imaging Group, 91–108.

Wang, S., M. V., de Hoop, and J., Xia, 2010, Acoustic inverse scattering via Helmholtz operator factorization and optimization: Journal of Computational Physics, **229**, 8445–8462, doi: https://doi.org/10.1016/j.jcp.2010.07.027.

Whitmore, N. D., and S., Crawley, 2012, Applications of RTM inverse scattering imaging conditions: 82nd Annual International Meeting, SEG, Expanded Abstracts, 1–6, doi: https://doi.org/10.1190/segam2012-0779.1.

Yu, J., J., Hu, G.T., Schuster, and R., Estill, 2006, Prestack migration deconvolution: Geophysics, **71**, no. 2, S53–S62, doi: https://doi.org/10.1190/1.2187783.